Visualization of vitamin A metabolism

Koenders, S.T.A.

Chapter 6

Visualizing Vitamin A Metabolism in the Small Intestines

Introduction

Retinoic acid (RA) is essential for embryonic development, cell differentiation and immunomodulation.[1,2] Its importance in immunology has already been recognized for 100 years.[3] In recent years the role of RA in the regulation of the immune system has been revisited and was shown to be important in the gut-homing of lymphocytes and function of dendritic cells (DCs).[4–6]

The precursors of RA, retinol (vitamin A) and β-carotene, are taken up from the diet by the epithelial cells of the small intestines.[7] These cells convert RA precursors into retinal. The next step, the conversion of retinal, which can be oxidized into RA by retinaldehyde dehydrogenases, such as ALDH1A1, ALDH1A2 and ALDH1A3 (**Fig. 6.1**).[8,9]

RA is required for the activation of DCs in the tissue of the small intestines.[10] RA binds to retinoic acid receptors (RAR), which modulate gene transcription and induce the expression of ALDH1A2 in DCs, thereby activating these cells.[10–12] As a result, the DCs are capable of producing RA by themselves. The activated DCs travel from the intestinal tissue to the gut-draining mesenteric lymph nodes, where they provide RA to lymphocytes (T and B cells).[10] RA induces the expression of the integrin α4β7 and the chemokine receptor CCR9 in the lymphocytes, which may bind to the mucosal vascular addressin cell adhesion molecule-1 (MadCAM-1) and the chemokine CCL25, respectively.[13,14] This process is termed the "imprinting of lymphocytes". Once the RA-imprinted lymphocytes leave the mesenteric lymph nodes, they travel through the bloodstream to find their interaction partners, which are expressed by the endothelial cells lining the vasculature of the small intestines. The RA-imprinted lymphocytes leave the bloodstream and enter the small intestines. The RA imprinting of lymphocytes by DCs therefore induces a gut-homing phenotype (**Fig. 6.1**).[5,6]

RA imprinted T and B cells undergo several cell-type specific changes. RA differentiates B cells into IgA plasma cells, which secrete IgA into the intestinal lumen. These cells are required for an effective control of the gut microbiome.[15] Activated T cells express Foxp3, which leads in the presence of TGF-β to the differentiation of T cells into immunosuppressive regulatory T (Treg) cells instead of the proinflammatory T helper 17 (Th17) cells.[16–19] RA controls, therefore, the balance between Treg and Th17 cells in the gut associated lymphoid tissue, which is crucial for immune homeostasis. An imbalance between Treg and Th17 cells may lead to autoimmune pathologies, such as inflammatory bowel disease, rheumatoid arthritis, multiple sclerosis and asthma, which can be characterized by an excess of Th17 cells.[4]

Currently, it is unknown which ALDH subtype is responsible for the production of RA required for the activation of DCs and the imprinting of the lymphocytes. Genetic deletion or pharmacological inhibition of these enzymes could shed light on this process. There are, however, no truly selective and potent ALDH inhibitors available[20] and constitutive genetic deletion of ALDH1A2 or ALDH1A3 is embryonically lethal.[21]

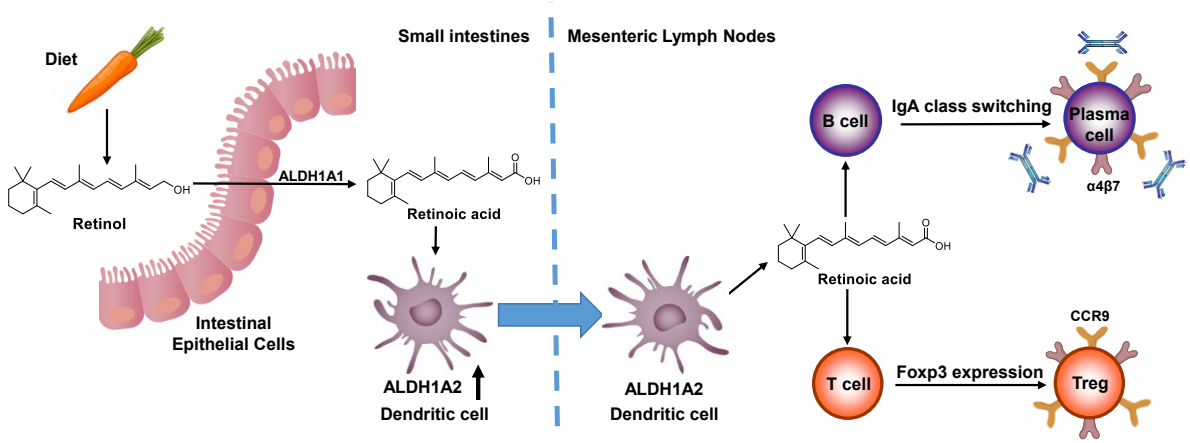

Fig. 6.1 | Schematic representation of the imprinting of DCs and lymphocytes by RA. On the left the uptake and conversion of retinol into RA by intestinal epithelial cells expressing ALDH1A1 is depicted. This results in a gradient of RA capable of imprinting DCs present in the underlying tissue of the small intestines. The retinoic acid binds to the nuclear retinoic acid receptor of the DCs and induces the expression of retinaldehyde dehydrogenase ALDH1A2. The activated DCs then travel to the mesenteric lymph nodes where they can provide T and B cells with the RA stimulus required for the expression of the gut-homing integrin α4β7 and chemokine receptor CCR9. Furthermore, the DCs stimulate T and B cells with RA to differentiate into IgA producing plasma cells and Foxp3 expressing Treg cells, respectively.

ALDH1A1 knock-out mice were viable, but did not display any significant phenotype, such as differences in Treg cells and fecal IgA levels (**Supplementary Fig. 6.1**).[22] This suggested that ALDH1A1 is not essential for the production of RA to activate DCs and to imprint lymphocytes. Of note, increased ALDH1A3 expression levels in the intestinal epithelial cells of vitamin A deficient mice have been previously described.[10] This may suggest that other aldehyde dehydrogenases (ALDHs) could be upregulated in the intestinal epithelial cells to compensate for the loss of ALDH1A1 in the knockout (KO) mice.

Activity-based protein profiling (ABPP) is a powerful chemical biological method that is ideally suited to report on the abundance and identity of active enzymes in complex biological systems.[23] It is a technology that relies on mechanism-based chemical probes that covalently and irreversibly react with the catalytic nucleophile in the active site of an enzyme in their native biological context.[24] Using the retinal-based probe, **LEI-945**[25], introduced and characterized in **chapters 3-5**, it was envisioned that retinaldehyde dehydrogenase activity could be identified and quantified in cell extracts derived from mouse intestines.

This chapter describes the development and application of a comparative ABPP method to profile the retinaldehyde dehydrogenase activities in intestinal cells derived from *Aldh1a1*^{WT} and *Aldh1a1*$^{-/-}$ mice. Chemical proteomics indicated that ALDH1B1 activity may contribute to the conversion of retinal into RA in the epithelial cells of the small intestines. Analysis of the ALDH1A1/ALDH1B1 double knock-out animals revealed a proinflammatory phenotype in which the gut-homing of Treg cells was significantly decreased. These data suggest that ALDH1B1 has retinaldehyde dehydrogenase activity, and is partly responsible for the production of RA in intestinal epithelial cells to induce Treg cells.

Results

Comparative ABPP of retinaldehyde dehydrogenases in intestinal epithelial cells derived from Aldh1a1^{WT} *mice and Aldh1a1*$^{-/-}$ *mice*

Since ALDH activity relies on a catalytic cysteine, which can be easily oxidized in non-cellular environments, chemical proteomics experiments were performed in intact cells to ensure a physiologically relevant readout. Freshly harvested epithelial cells from the small intestines and cells from the mesenteric lymph nodes of wild type mice were treated with **LEI-945** (1 µM, 1 h), washed, pelleted and snap frozen until the proteomics experiment was performed. The same procedure for label-free quantification (LFQ) proteomic analysis was followed as described in **Chapters 4** and **5**. In short, the cells were thawed, lysed in MilliQ and subjected to Copper(I)-catalyzed alkyne-azide [2+3] cycloaddition with a biotin-azide. Incubation with avidin beads, followed by several washing steps, tryptic digestion, desalting and analysis using LC-MS/MS. This chemical proteomics experiment resulted in the detection of over 300 proteins.

ALDH1A1, ALDH1A7, ALDH1B1, ALDH2 and ALDH3A2 were significantly enriched in the intestinal epithelial cells (**Fig. 6.2a**), whereas ALDH1A2, ALDH2 and ALDH3A2 were identified in cells from the mesenteric lymph nodes (**Fig. 6.2b**). Based on the previously reported tissue distribution of ALDHs in mice, this subset covers all the ALDHs expressed in the intestinal cells of mice.[26] An overview of all significantly enriched enzymes in the wild type intestinal cells is shown in **Supplementary Tables 6.1** and **6.2**.

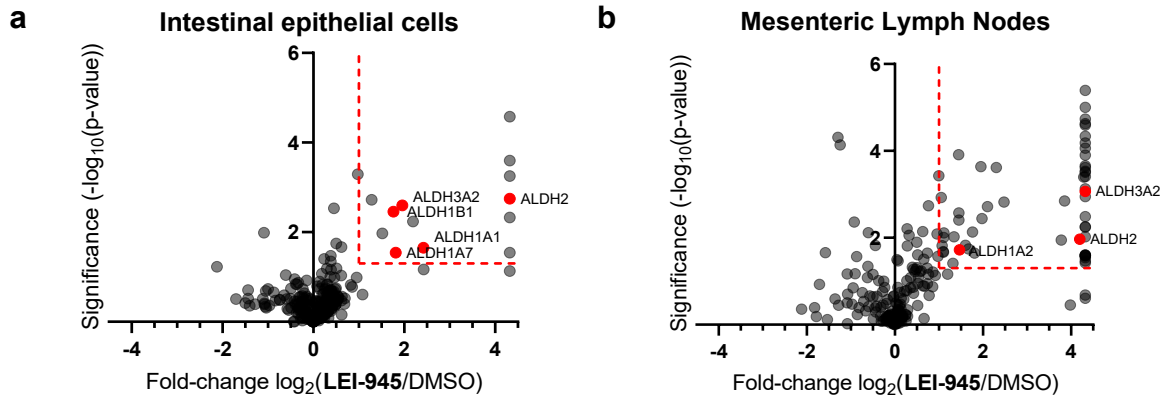

Fig. 6.2 | Chemical proteomics data of ALDH enzymes intestinal cells derived from wild type mice. **a**, Volcano plot for total proteins identified in a chemical proteomics experiment with probe **LEI-945** (1 µM) in intestinal epithelial cells (IEC). Red lines indicate threshold values marking significantly enriched (fold-change > 2; p-value < 0.05) proteins. Red dots represent significantly enriched ALDH enzymes. **b**, Volcano plot for total proteins identified in a chemical proteomics experiment with probe **LEI-945** (1 µM) in mesenteric lymph node (MLN) cells. Red lines indicate threshold values marking significantly enriched (fold-change > 2; p-value < 0.05) proteins. Red dots represent significantly enriched ALDH enzymes. For parts **a** and **b**, data are from $N = 4$ experiments (biological replicates).

To determine which retinaldehyde dehydrogenase may compensate for the loss of ALDH1A1 activity in the small intestines of *Aldh1a1*$^{-/-}$ mice, a comparative chemical proteomics experiment using **LEI-945** was performed using epithelial cells from *Aldh1a1*^{WT} and *Aldh1a1*$^{-/-}$ mice. To this end, the LFQ values of ALDHs from *Aldh1a1*^{WT} and *Aldh1a1*$^{-/-}$ mice were determined (**Fig. 6.3a**). Chemical proteomics confirmed that the knockout mice did not show any ALDH1A1 activity. Of note, the levels of active ALDH1A7, a mouse specific isozyme, which cannot convert retinal into retinoic acid[26,27], were also decreased in the intestinal epithelial cells from the *Aldh1a1*$^{-/-}$ mice. This is in line with a previous report in which the loss of ALDH1A7 activity was attributed to their adjacent genetic localization on chromosome 19.[28] The levels of ALDH1B1 activity had notably increased in the *Aldh1a1*$^{-/-}$ mice, whereas the levels of ALDH2 and ALDH3A2 were unchanged. ALDH1B1 and ALDH2 were the most abundant ALDH activities in intestinal epithelial cells.

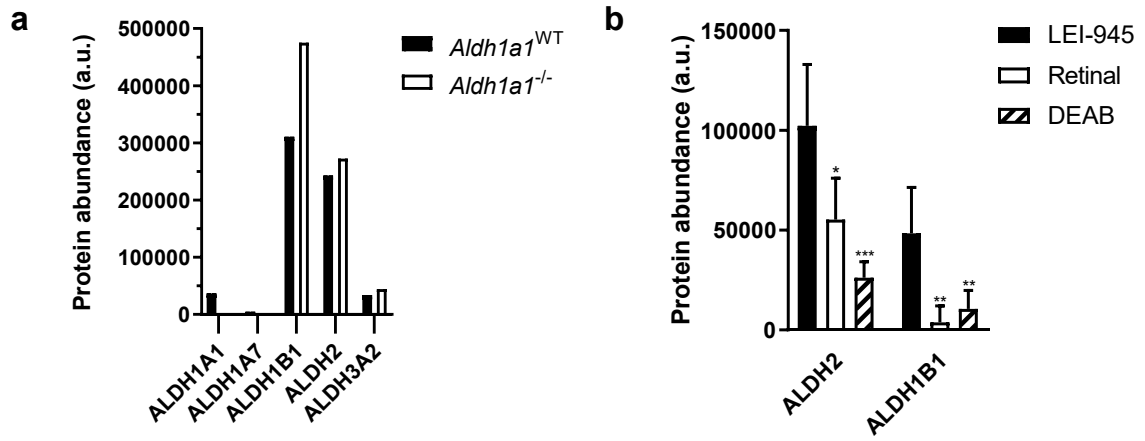

Fig. 6.3 | Comparative and competitive ABPP of ALDH enzymes in intestinal epithelial cells. a, Data represent mean LFQ values for ALDHs significantly enriched in intestinal epithelial cells derived from *Aldh1a1*^{WT} and *Aldh1a1*$^{-/-}$ mice. Data are from $N \geq 1$ experiments (biological replicates). **b**, Competitive ABPP data from competition of retinal (30 μM) or DEAB (30 μM) with **LEI-945** (1 μM) in mouse intestinal epithelial cells. Data represent mean LFQ values ± SD; $N = 4$ experiments (biological replicates). P* < 0.05, P** < 0.01 and P*** < 0.001; *t* test, two-sided.

Competitive ABPP experiments with general ALDH inhibitor 4-diethylaminobenzaldehyde (DEAB) and the natural substrate retinal were performed to exclude non-specific labeling (**Fig. 6.3b**). Competitive ABPP with DEAB showed a significant decrease in labeling for ALDH1B1 and ALDH2, whereas competition with retinal showed a significant, but small (less than 50%) inhibition of ALDH2, while ALDH1B1 showed almost complete inhibition by the natural substrate (**Fig. 6.3b**).

Since ALDH2 is unable to convert retinal[29,30], it is considered an unlikely candidate to compensate for the loss of ALDH1A1 activity. Although acetaldehyde was previously described as the main substrate of ALDH1B1[31], retinal can also serve as a substrate for recombinant human ALDH1B1 in *in vitro* assays.[30] Of note, ALDH1B1 is primarily expressed in the small intestines[26] and upregulated in mice fed a high fiber diet in a similar fashion as ALDH1A1 (data not shown).[8] Of the ALDHs identified using ABPP, ALDH1B1 has one of the highest levels of active enzyme in mouse epithelial cells. Together, these data suggest a possible tissue specific role of ALDH1B1 in RA synthesis and immune homeostasis and that it could compensate for the loss of ALDH1A1.

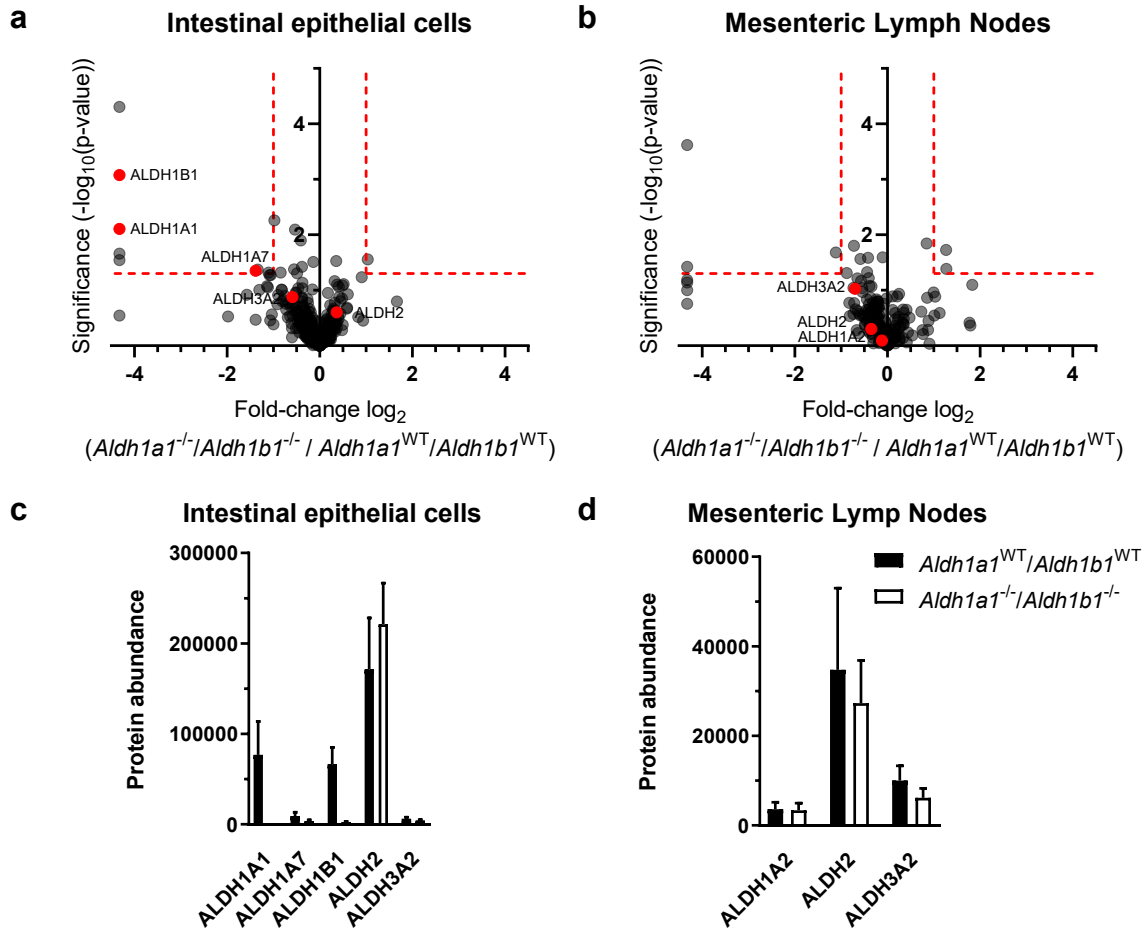

Fig. 6.4 | Comparative ABPP of ALDHs in intestinal cells derived from *Aldh1a1*^{WT}/*Aldh1b1*^{WT} and *Aldh1a1*$^{-/-}$/*Aldh1b1*$^{-/-}$ mice. a, Volcano plot for total proteins identified in chemical proteomics experiment with probe **LEI-945** (1 µM) comparing intestinal epithelial cells derived from *Aldh1a1*^{WT}/*Aldh1b1*^{WT} with *Aldh1a1*$^{-/-}$/*Aldh1b1*$^{-/-}$ mice. Red lines indicate threshold values marking significantly enriched (fold-change > 2; p-value < 0.05) proteins. Red dots represent significantly enriched ALDH enzymes. **b**, Volcano plot for total proteins identified in chemical proteomics experiment with probe **LEI-945** (1 µM) comparing cells derived from the mesenteric lymph nodes of *Aldh1a1*^{WT}/*Aldh1b1*^{WT} and *Aldh1a1*$^{-/-}$/*Aldh1b1*$^{-/-}$ mice. Red lines indicate threshold values marking significantly enriched proteins. Red dots represent significantly enriched ALDH enzymes. **c**, Protein abundance of ALDHs. Data represent mean LFQ values ± SD for significantly enriched ALDHs in intestinal epithelial cells derived from *Aldh1a1*^{WT}/*Aldh1b1*^{WT} or *Aldh1a1*$^{-/-}$/*Aldh1b1*$^{-/-}$ mice. **d**, Protein abundance of ALDHs. Data represent mean LFQ values ± SD for significantly enriched ALDHs in cells derived from the mesenteric lymph nodes of *Aldh1a1*^{WT}/*Aldh1b1*^{WT} and *Aldh1a1*$^{-/-}$/*Aldh1b1*$^{-/-}$ mice. For parts **a-d**, $N = 4$ experiments (biological replicates).

Aldh1a1$^{-/-}$*/Aldh1b1*$^{-/-}$ *mice display a more proinflammatory phenotype*

ALDH1B1 has not yet been studied in the context of gut-homing and immune homeostasis. To determine whether ALDH1B1 plays a role in the regulation of the immune system within the small intestines, mice deficient for both *Aldh1a1* and *Aldh1b1* genes were investigated. Chemical proteomics using **LEI-945** confirmed the epithelial cells derived from the small intestines of these transgenic mice were indeed lacking ALDH1A1 and ALDH1B1 activity (**Fig. 6.4a,c**).

Furthermore, the ABPP analysis indicated that the activity of ALDH2 and ALDH3A2 did not change significantly, while ALDH1A7 activity was decreased (**Fig 6.4a,c**). ALDH1A2, ALDH2 and ALDH3A2 were detected in cells derived from the mesenteric lymph nodes (**Fig. 6.4b,c**). The ALDHs detected in the mesenteric lymph nodes, did not show any significant change in activity in the double-knockout compared with the wild type.

To determine whether *Aldh1a1*$^{-/-}$*/Aldh1b1*$^{-/-}$ mice did display an altered phenotype, the amount of Treg cells, activated DCs and IgA levels were measured. The presence of Treg cells in *Aldh1a1*$^{-/-}$*/Aldh1b1*$^{-/-}$ mice was determined within the tissue of the intestines using fluorescence-activated cell sorting (FACS). A significant decrease in the frequency of Foxp3^{+}CD25^{+} Treg cells was detected (**Fig. 6.5a**). This decrease in immunosuppressive Treg cells was accompanied by an increase of CD45^{+} leukocytes within the epithelium (**Fig. 6.5b**). There was no change in the amount of activated DCs present (**Fig. 6.5c,d**). Of note, the amount of IgA in the lumen was also significantly increased (**Fig. 6.5e**). These data suggest that the combined absence of ALDH1A1 and ALDH1B1 proteins leads to a shift in the immune homeostasis of the small intestines towards a proinflammatory phenotype.

Discussion

The hypothesis that production of RA by the intestinal epithelial cells required for the effective imprinting of dendritic cells depends on ALDH1A1 activity, was previously contested by a lack of disruption in the immune homeostasis in *Aldh1a1*$^{-/-}$ mice. To investigate which ALDH enzyme could compensate for the loss of ALDH1A1 activity, comparative ABPP using **LEI-945** in intestinal epithelial cells derived from wild type and ALDH1A1 knockout mice was performed. High levels of ALDH1B1 and ALDH2 activity were identified in the intestinal epithelial cells.

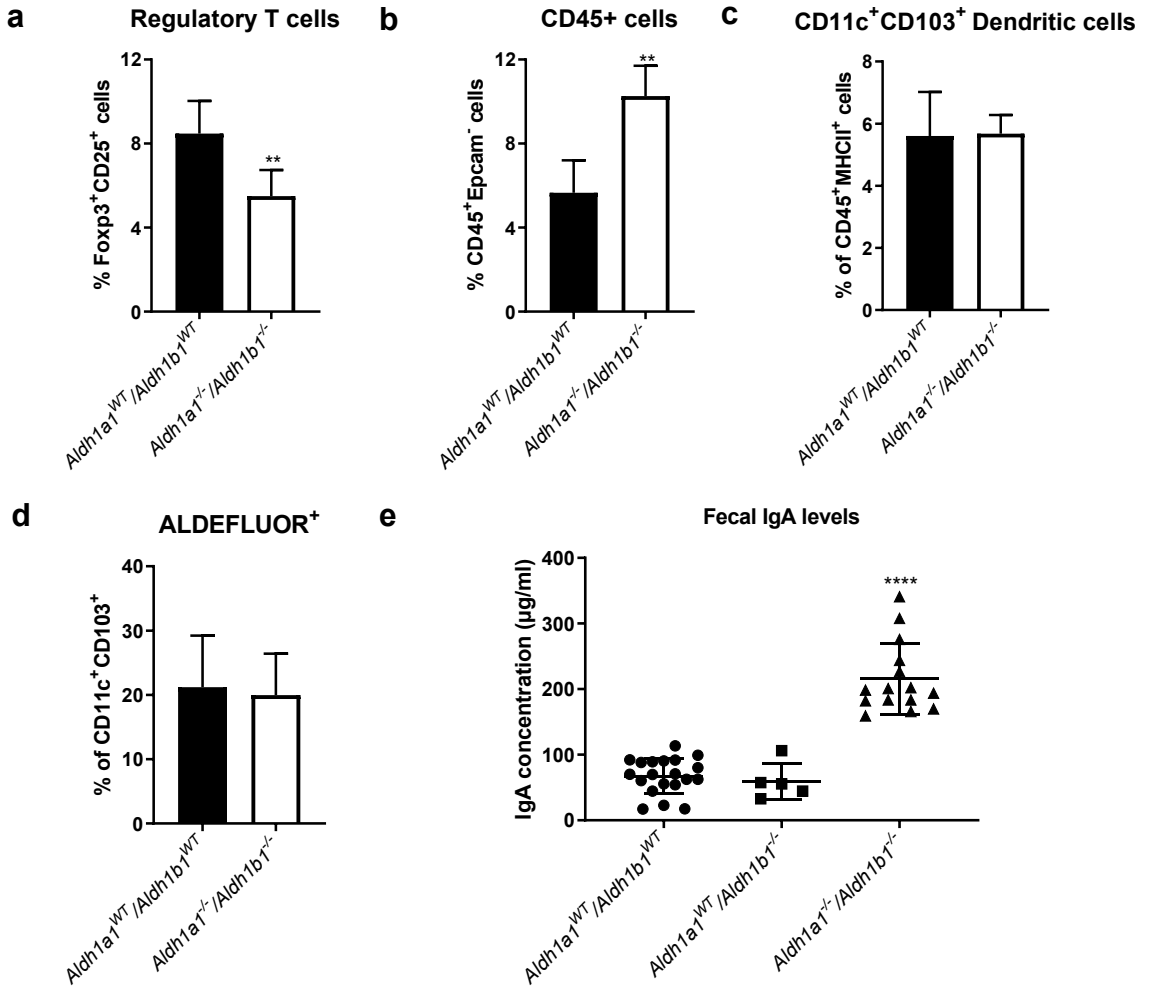

Fig. 6.5 | *Aldh1a1*$^{-/-}$/*Aldh1b1*$^{-/-}$ mice display a more proinflammatory phenotype. a, Graph showing the proportion of regulatory T cells (Foxp3^{+}CD25^{+}) in CD45^{+}CD3^{+}CD4^{+} T cells. Data represent mean values ± SD; *N* = 6 experiments (biological replicates). **P < 0.01; Mann-Whitney test; two-tailed. **b**, Graph showing the proportion of leukocytes (CD45^{+}) in the small intestinal epithelial layer. Data represent mean values ± SD; *N* = 5 experiments (biological replicates). **P < 0.01; Mann-Whitney test, two-tailed. **c**, Graph showing the proportion of CD11c^{+}CD103^{+} dendritic cells in CD45^{+}MHCII^{+} cells. **d**, Graph showing the proportion of ALDEFLUOR^{+} cells in CD11c^{+}CD103^{+} dendritic cells. For parts **c** and **d**, data represent mean values ± SD; *N* = 4 experiments (biological replicates). **e**, Graph showing the amount of IgA in the lumen of *Aldh1a1*^{WT}/*Aldh1b1*^{WT}, *Aldh1a1*^{WT}/*Aldh1b1*$^{-/-}$ and *Aldh1a1*$^{-/-}$/*Aldh1b1*$^{-/-}$ mice. Data represent mean values ± SD; N = 14. ****P < 0.0001; Mann-Whitney test, two-tailed.

However, the probe labelling of ALDH1B1 could be efficiently competed with retinal, whereas labelling of ALDH2 only decreased modestly. This suggested that ALDH1B1 could be an alternative enzyme capable of producing RA in the small intestines.

To date, the role of ALDH1B1 in immune homeostasis has not been investigated, therefore the gut-homing of lymphocytes in transgenic mice lacking both *Aldh1a1* and *Aldh1b1* genes was studied. FACS analysis of the immune cell populations in the small intestines of these mice showed a lymphocyte composition corresponding with a more proinflammatory phenotype.

Chemical proteomics experiments on intestinal cells derived from the *Aldh1a1*$^{-/-}$/*Aldh1b1*$^{-/-}$ mice showed no changes in the levels of other ALDHs to compensate for the loss of ALDH activity. There was also no alteration in the amount of ALDH1A2 activity in the mesenteric lymph nodes, corresponding with the observation of unchanged levels of DCs with high ALDH activity or ALDEFLUOR^{+} DCs. Therefore, only the ALDH activity in the epithelial layer seems to be directly affected by the *Aldh1a1*$^{-/-}$/*Aldh1b1*$^{-/-}$ knockout.

Although the *Aldh1a1*$^{-/-}$/*Aldh1b1*$^{-/-}$ knockout mice did show a proinflammatory phenotype, only the expected decrease in the amount of Treg cells was observed. The amount of activated DCs was not affected and IgA levels increased, while a decrease of both was expected as a result of lower RA levels. Several factors might be considered in order to explain these seemingly contradictory results: retinoid levels, composition of the gut microbiome and short-chain fatty acid (SCFA) levels.

In a recent study it has been shown that the gut microbiome influences vitamin A metabolism by subduing retinol dehydrogenase 7 (*Rdh7*) expression in intestinal epithelial cells.[32] Suppressing the levels of Rdh7, which converts retinol into retinal, lowered the formation of RA locally in the epithelial layer. As a result, the conversion of retinol shifted to the production of retinyl esters for storage in the liver, while retinaldehyde dehydrogenase levels remained unchanged.[32] This shift is favourable to commensal bacteria as RA enhances the production of IL-22, which supports epithelial integrity and the antimicrobial response via the production of antimicrobial peptides, such as Reg3β and Reg3γ.[33] A knockout of Rdh7 led to 3-fold lower levels of RA and a reduction of IL-22, Reg3β and Reg3γ.[32] However, in the *Aldh1a1*$^{-/-}$/*Aldh1b1*$^{-/-}$ mice no significant alteration in the levels of these antimicrobial markers was detected (data not shown).

This beckons the question to what extent the retinoid levels in the intestinal tissue of the knockout mice have changed and whether the observed changes are due to a change in RA levels or affect the intestinal environment in other ways. To answer these questions the actual levels of RA in the intestinal tissues of these mice will have to be measured. Additionally, the LC-UV/MS assay introduced in **Chapter 4** could be used to determine the ability of intestinal epithelial cells derived from wild type and knockout mice to convert retinal into RA.

Nonetheless, there was a significant reduction in the proportion of Treg cells in the intestinal tissue of *Aldh1a1*$^{-/-}$/*Aldh1b1*$^{-/-}$ mice. The decrease in Treg cells was also accompanied by an increase of leukocytes in the epithelium. This phenotype resembles that of pathologies such as coeliac disease.[34] However, the previously proposed model of disrupted activation of DCs resulting in less Treg cells, cannot explain this observed reduction as no difference in DC subsets in the mesenteric lymph nodes were observed. A more detailed characterization of the leukocytes in the epithelial layer of *Aldh1a1*$^{-/-}$/*Aldh1b1*$^{-/-}$ mice might provide insight into the factors influencing the observed changes.

Remarkably, an increase in fecal IgA levels was detected instead of the expected decrease due to reduced lymphocyte recruitment. A possible explanation might be found in the composition of the gut microbiome. A balanced gut microbiome is essential for immune homeostasis as germ free mice are ineffective at sustaining Tregs.[35] This has been linked to the short-chain fatty acids (SCFAs), such as acetate, propionate and butyrate, produced by commensal bacteria from dietary fiber.[8,36–38] SCFAs can effect gut homeostasis via two pathways: histone deacetylase inhibition and binding to G-protein-coupled receptors, such as GPR43 and GPR109a.[39] Propionate and butyrate can inhibit histone deacetylases, inducing ALDH1A2 expression in dendritic cells and Foxp3 expression in T cells[8,38], whereas binding of acetate to GPR43 induces ALDH1A2 expression in dendritic cells and an increase of IgA production in B cells.[40]

Changes in the composition of the gut microbiome or an aberrant reaction to the microbiome, are therefore other factors to be considered. However, SCFA levels and the composition of the bacteria making up the gut microbiome have not been determined in this study. These could provide an answer for the discrepancy between the expected decrease in IgA producing plasma cells and the detected increase in fecal IgA.

Conclusion

ABPP with **LEI-945** was capable of determining the levels of active ALDH enzymes in intestinal cells derived from mice. This shows that **LEI-945** can not only be used for the profiling of ALDHs in cultured (cancer) cell lines, but also in primary material *ex vivo*. Using both comparative and competitive ABPP, ALDH1B1 was identified as a potential enzyme contributing to the production of RA in the small intestines. *Aldh1a1*$^{-/-}$/*Aldh1b1*$^{-/-}$ mice showed a proinflammatory phenotype with an influx of leukocytes in the epithelium, a decrease in Treg cells and higher levels of fecal IgA.

Acknowledgements

Martje Erkelens is kindly acknowledged for harvesting the intestinal cells from mice, performing the FACS assays, her collaboration on preparing the proteomics samples and helpful discussions. Bogdan Florea is acknowledged for mass spectrometry analysis.

Experimental procedures

Biological methods

Materials, probe and inhibitors. Activity-based probe **LEI-945** was synthesized in-house as previously described in **Chapter 3**. DEAB and retinal were purchased from Sigma Aldrich.

Mice. *Aldh1a1* deficient mice[14] were obtained from The Jackson Laboratory, USA (stock #012247), and were bred heterozygous x heterozygous so both wild type and knock out animals were available from the same litter. Both male and female mice were used aged 6-20 weeks. Mice were housed under specific pathogen free conditions at the VU University Animal Facility. All experiments have been approved by the VU University Scientific and Animal Ethics Committees according to Dutch law. *Aldh1a1/1b1* deficient mice were created at Yale University and experiments were performed with age matched wild type animals. Mice were housed under specific pathogen free conditions at the Yale University Animal Facility, New Haven, CT USA. At the time of the experiments all mice were aged 8-12 weeks and experiments were performed in accordance with local ethical regulations.

Ex vivo single cell suspensions. Small intestines and mesenteric lymph nodes were dissected from mice and fatty tissue was removed as much as possible. Luminal contents were collected in 1 ml PBS and stored at -20 °C. Then, intestines were opened longitudinally and washed in phosphate-buffered saline without calcium (D-PBS) (Gibco, Life Technologies, Paisley, United Kingdom) to remove all fecal contents. To isolate intestinal epithelial cells, the intestines were transferred to 1x Hank's Balanced Salt Solution (HBSS) (Invitrogen, Breda, The Netherlands) containing 5% Fetal Calf Serum (FCS) (HyClone Laboratories/Greiner Bio-One, Alphen aan den Rijn, The Netherlands) and 2.5 mM EDTA (Sigma Aldrich, Zwijndrecht, The Netherlands) and incubated on ice for 30 minutes. Tissues were vortexed vigorously for the removal of epithelial cells. The remaining tissue and the mesenteric lymph nodes were minced and incubated separately while constantly stirring for 30 minutes in 37 °C in HBSS + 5% FCS + 0,5 mM collagenase IV (Roche, Penzberg, Germany) in order to obtain a single cell suspension of both the lamina propria and the mesenteric lymph nodes. The lamina propria suspension was filtered through a 70 µm cell-strainer (BD Biosciences, Breda, The Netherlands) and washed once with HBSS containing 5% FCS. Suspensions were either used for FACS analysis or ABPP.

Flow cytometry. The ALDEFLUOR assay kit (StemCell Technologies, Grenoble, France) was used to measure ALDH activity using flow cytometry according to the manufacturer's protocol. In some cases cells were incubated with an increasing series of retinal (Sigma Aldrich, Zwijndrecht, the Netherlands) as a competitive substrate while the ALDEFLUOR assay was performed. Subsequently, cells were stained with anti-Epcam-PE, anti-CD45-PE-Cy7, anti-CD11c e450 (eBioscience, Amsterdam, the Netherlands), anti-MHCII 647, anti-CD103-biotin (BD Bioscience, Breda, The Netherlands), and Streptavidin eFluor 605NC (both eBioscience, Amsterdam, the Netherlands). anti-podoplanin (clone GP38, made in house), anti-CD45-viogreen (Miltenyi Biotec, Leiden, The Netherlands), anti-CD31-PE-Cy7 (eBioscience, Amsterdam, the Netherlands) and goat-anti-hamster 647 (Invitrogen, Landsmeer, the Netherlands). 7-AAD (Thermo Fisher Scientific, Breda, The Netherlands), and DAPI (Invitrogen, Landsmeer, the Netherlands) were used to discriminate between live and death cells. Cells were analyzed with LSR Fortessa X-20 (BD care, Erembodegeme, Belgium). Data was analyzed using FlowJo software (Tree Star, Ashland, OR, USA).

Enzyme-linked immunosorbent assay (ELISA) for secretory IgA. Collected luminal contents were thawed and shaken at 4 °C for 60 minutes to homogenize the samples. Then, samples were centrifuged at maximum speed for 5 minutes to remove the debris and supernatant was collected for analysis by ELISA. Plates were coated with anti-mouse-IgA antibody to capture secretory IgA or mouse-IgA used as a standard (clone s107), followed by anti-mouse-IgA-biotin (all Southern Biotech, Birmingham, AL, USA) antibody, and subsequently streptavidin labeled with HRP (Thermo Fischer Scientific, Landsmeer, the Netherlands). Samples were analyzed with a Fluostar Optima microplate reader (BMG Labtech, Isogen Lifescience, De Meern, the Netherlands).

Ex vivo activity-based proteomics

Sample preparation for chemical proteomics. Protocol adapted from previously described procedure.[41] Cells were treated with vehicle or **LEI-945** (1 µM) in PBS. In the case of competitive ABPP vehicle, DEAB (100 µM) or retinal (100 µM) was added. After 1 hour cells were washed, snap frozen and stored at -20 °C. When required cells were thawed, lysed and adjusted to 1 mg/mL protein concentration as determined by a Quick Start™ Bradford Protein assay (Bio-Rad). 250 µL was taken from each sample and to this 25 µL freshly prepared "click" mixture containing 1 mM $CuSO_4$ (2.5 µL/sample, 100 mM in H_2O), 5 mM NaAsc (1.25 µL/sample, 1 M in H_2O), 0.4 mM THPTA (1 µL/sample, 100 mM in DMSO), 40 µM biotin-N_3 (2.5 µL/sample, 4 mM in DMSO) and MilliQ (17.75 µL/sample) was added. Samples were incubated for 1 hour at 37 °C while shaking (300 rpm). Excess click reagents were then removed by chloroform/methanol precipitation followed by another wash with methanol. Precipitated proteomes were then suspended in urea buffer (250 µL, 6 M urea and 25 mM ammonium bicarbonate), DTT (2.5 µL, 1 M) was added and the mixture was then incubated for 15 min at 65 °C while shaking (600 rpm). The samples were then allowed to cool down to RT and then alkylated by addition of iodoacetamide (20 µL, 0.5M) for 30 minutes at RT in the dark. Addition of SDS (70 µL, 10% (v/v)) was followed by heating at 65 °C for 5 minutes. For each sample 50 µL 50% slurry of Avidin-Agarose from egg white (Sigma-Aldrich) was washed three times with PBS and transferred in PBS (1 L) to a 15 mL tube. To this another 2 mL of PBS was added followed by the corresponding proteome sample. The beads were incubated with the proteome for 2 hours at room temperature using an overhead shaker. The beads were then isolated by centrifugation (2 min, 2500 g), washed with SDS in PBS (0.5% (w/v)) and washed three times with PBS. The beads were then transferred to low-binding Eppendorf tubes and proteins were digested overnight at 37 °C and 950 rpm in 250 µL digestion buffer (100 mM Tris, 100 mM NaCl, 1 mM $CaCl_2$, 2% acetonitrile and 0.5 µg sequencing grade trypsin (Promega)). Digestion was stopped by addition of formic acid (12.5 µL) and the beads filtered off by centrifugation (2 min, 600 g) using a Bio-Spin column (Bio-Rad). Samples were then desalted using stage tips, collected in low-binding Eppendorf tubes, concentrated using a SpeedVac (Eppendorf) and stored at -20 °C until reconstitution before measurement.[42]

LC-MS/MS measurement and analysis. Samples were reconstituted in LC-MS sample solution (50 µL, MilliQ, 3% acetonitrile/ 0.1% formic acid/20 fmol/µL enolase). Samples were then analysed using a NanoACQUITY UPLC System (Waters) coupled to a SYNAPT G2-Si high-definition mass spectrometer (Waters) as previously described.[41,43] Of each sample 5 µL was loaded on a nanoEASE™ M/Z Symmetry C18 trap column (particles 5 µm, 100 Å , 180 µm x 20 mm, Waters) with 0.1% formic acid and separated on an nanoEASE™ M/Z HSS C18 T3 analytical column (particles 1.8 µm, 75 µm x 250 mm, Waters) heated at 80 °C. A multistep gradient running from 5-40% acetonitrile containing 0.1% formic acid during a 70 minute method at 300 nL/min was used to achieve peptide separation. Survey scans (m/z 50-2000 Da) were acquired in the Synapt with a scan time of 0.6 seconds in positive, resolution mode. The collision energy is set to 4 V in the trap cell for low-energy MS mode. For the elevated energy scan, the transfer cell collision energy is ramped using drift-time specific collision energies. The lock mass is sampled every 30 seconds. MS raw files were analysed with ProteinLynx Global SERVER (PLGS, v3.0.3, Waters). The MS^E identification was also performed with PLGS using the human proteome from Uniprot (Uniprot-homo-sapiens-trypsin-reviewed-2016-08-29.fasta). The following parameter settings were used: low energy threshold 150 counts, elevated energy threshold 30, peptide and protein FDR 1%, enzyme specificity trypsin, max missed cleavages max 2, variable modification methionine oxidation, fixed modification carbamidomethylation cysteine, at least: fragments/peptide 2, fragments/protein 5, peptides/protein 1 and number of peptides to measure per protein 3. For label-free quantification ISOQuant (v1.5) was used.[44,45] Data were filtered to retain only proteins with two or more reported unique peptides and quantified in at least 3 replicates of the positive control (probe-treated). Proteins were designated as significantly enriched by the probe when they showed 2-fold enrichment in quantification value when comparing negative control (vehicle-treated) with positive control (probe-treated) samples and probability as determined by a Student's *t* test (<0.05).

Supplementary Data

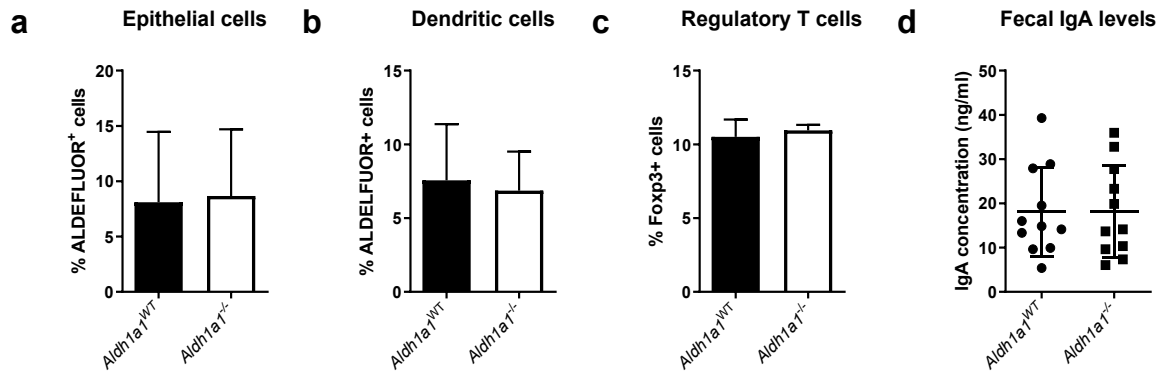

Supplementary Fig. 6.1 | *Aldh1a1*$^{-/-}$ mice show no change in immune homeostasis. a, Graph showing the proportion of ALDEFLUOR^{+} cells in the small intestine epithelial layer. **b**, Graph showing the proportion of ALDEFLUOR^{+} cells in dendritic (CD45^{+}MHCII^{+}CD11c^{+}CD103^{+}) cells. For parts **a** and **b**, data represent mean values ± SD; N = 7 experiments (biological replicates). **c**, Graph showing the proportion of Foxp3^{+} cells in T cells. Data represent mean values ± SD; N = 4 experiments (biological replicates). **d**, Graph showing the amount of IgA in the lumen of *Aldh1a1*^{WT} and *Aldh1a1*$^{-/-}$ mice. Data represent mean values ± SD; N = 11 experiments (biological replicates).

Supplementary Table 6.1 | Proteins significantly enriched using LEI-945 (1 µM) in intestinal epithelial cells derived from *Aldh1a1*^{WT} mice corresponding to Fig. 6.2a.

Name	Gene name	Accession	Uniprot ID	Fold-change	Significance ($-\log_{10}$)
Heat shock 70 kDa protein 1A	Hspa1a	Q61696	HS71A_MOUSE	20.0	3.6
Aldehyde dehydrogenase_ mitochondrial	Aldh2	P47738	ALDH2_MOUSE	20.0	2.7
Thioredoxin-related transmembrane protein 1	Tmx1	Q8VBT0	TMX1_MOUSE	20.0	4.6
Voltage-dependent anion-selective channel protein 1	Vdac1	Q60932	VDAC1_MOUSE	20.0	3.3
Voltage-dependent anion-selective channel protein 3	Vdac3	Q60931	VDAC3_MOUSE	20.0	2.3
Keratin_ type II cytoskeletal 72	Krt72 PE	Q6IME9	K2C72_MOUSE	20.0	1.5
Retinal dehydrogenase 1	Aldh1a1	P24549	AL1A1_MOUSE	5.4	1.7
Protein disulfide-isomerase	P4hb	P09103	PDIA1_MOUSE	4.6	2.2
Fatty aldehyde dehydrogenase	Aldh3a2	P47740	AL3A2_MOUSE	3.9	2.6
Aldehyde dehydrogenase_ cytosolic 1	Aldh1a7	O35945	AL1A7_MOUSE	3.5	1.5
Aldehyde dehydrogenase X_ mitochondrial	Aldh1b1	Q9CZS1	AL1B1_MOUSE	3.4	2.5
Mitochondrial carrier homolog 2	Mtch2	Q791V5	MTCH2_MOUSE	2.9	2.0
Cytochrome b5 type B	Cyb5b	Q9CQX2	CYB5B_MOUSE	2.4	2.7

Supplementary Table 6.2 | Proteins significantly enriched using LEI-945 (1 µM) in mesenteric lymph nodes derived from *Aldh1a1*^{WT} mice corresponding to Fig. 6.2b.

Name	Gene name	Accession	Uniprot ID	Fold-change	Significance ($-\log_{10}$)
Stimulator of interferon genes protein	Tmem173	Q3TBT3	STING_MOUSE	20.0	1.5
Fructose-bisphosphate aldolase A	Aldoa	P05064	ALDOA_MOUSE	20.0	4.1
Tubulin beta-2A chain	Tubb2a	Q7TMM9	TBB2A_MOUSE	20.0	4.3
14-3-3 protein theta	Ywhaq	P68254	1433T_MOUSE	20.0	1.6
40S ribosomal protein S18	Rps18	P62270	RS18_MOUSE	20.0	1.6
Acetyl-CoA acetyltransferase_ mitochondrial	Acat1	Q8QZT1	THIL_MOUSE	20.0	1.6
Estradiol 17-beta-dehydrogenase 11	Hsd17b11	Q9EQ06	DHB11_MOUSE	20.0	3.1
Fatty aldehyde dehydrogenase	Aldh3a2	P47740	AL3A2_MOUSE	20.0	3.1
Glutamate dehydrogenase 1_ mitochondrial	Glud1	P26443	DHE3_MOUSE	20.0	4.6
Proteasome activator complex subunit 2	Psme2	P97372	PSME2_MOUSE	20.0	3.9
Extended synaptotagmin-2	Esyt2	Q3TZZ7	ESYT2_MOUSE	20.0	4.7
40S ribosomal protein SA	Rpsa	P14206	RSSA_MOUSE	20.0	1.6
Sideroflexin-3	Sfxn3	Q91V61	SFXN3_MOUSE	20.0	3.5
Immunity-related GTPase family M protein 1	Irgm1	Q60766	IRGM1_MOUSE	20.0	3.5
Elongation factor 1-gamma	Eef1g	Q9D8N0	EF1G_MOUSE	20.0	1.5
60S ribosomal protein L5	Rpl5	P47962	RL5_MOUSE	20.0	1.4
Voltage-dependent anion-selective channel protein 2	Vdac2	Q60930	VDAC2_MOUSE	20.0	3.4
Voltage-dependent anion-selective channel protein 3	Vdac3	Q60931	VDAC3_MOUSE	20.0	2.9
Inactive hydroxysteroid dehydrogenase-like protein 1	Hsdl1	Q8BTX9	HSDL1_MOUSE	20.0	2.3
H-2 class II histocompatibility antigen gamma chain	Cd74	P04441	HG2A_MOUSE	20.0	2.0
Cytochrome b5 type B	Cyb5b	Q9CQX2	CYB5B_MOUSE	20.0	2.2
Thioredoxin-related transmembrane protein 1	Tmx1	Q8VBT0	TMX1_MOUSE	20.0	2.5
Voltage-dependent anion-selective channel protein 1	Vdac1	Q60932	VDAC1_MOUSE	20.0	3.7
40S ribosomal protein S2	Rps2	P25444	RS2_MOUSE	20.0	5.4
60S ribosomal protein L17	Rpl17	Q9CPR4	RL17_MOUSE	20.0	4.6
40S ribosomal protein S5	Rps5	P97461	RS5_MOUSE	20.0	5.0
Triosephosphate isomerase	Tpi1	P17751	TPIS_MOUSE	20.0	4.2
Aconitate hydratase_ mitochondrial	Aco2	Q99KI0	ACON_MOUSE	20.0	1.6
Hemoglobin subunit beta-2	Hbb-b2	P02089	HBB2_MOUSE	20.0	3.6
Delta(14)-sterol reductase	Lbr	Q3U9G9	LBR_MOUSE	19.5	3.4
Aldehyde dehydrogenase_ mitochondrial	Aldh2	P47738	ALDH2_MOUSE	18.3	2.0
ADP/ATP translocase 2	Slc25a5	P51881	ADT2_MOUSE	14.4	2.8
Mitochondrial carrier homolog 2	Mtch2	Q791V5	MTCH2_MOUSE	13.7	1.9
Phosphate carrier protein_ mitochondrial	Slc25a3	Q8VEM8	MPCP_MOUSE	5.6	2.8
Guanine nucleotide-binding protein G(i) subunit alpha-2	Gnai2	P08752	GNAI2_MOUSE	4.9	3.6
ADP/ATP translocase 1	Slc25a4	P48962	ADT1_MOUSE	4.3	2.7
Tubulin alpha-1C chain	Tuba1c	P68373	TBA1C_MOUSE	3.9	2.4
Ubiquitin-40S ribosomal protein S27a	Rps27a	P62983	RS27A_MOUSE	3.9	3.6
Glyceraldehyde-3-phosphate dehydrogenase	Gapdh	P16858	G3P_MOUSE	3.5	1.6
Tubulin alpha-4A chain	Tuba4a	P68368	TBA4A_MOUSE	3.4	2.1
L-lactate dehydrogenase A chain	Ldha	P06151	LDHA_MOUSE	3.2	1.7
Plastin-2	Lcp1	Q61233	PLSL_MOUSE	3.0	1.8
Retinal dehydrogenase 2	Aldh1a2	Q62148	AL1A2_MOUSE	2.8	1.7
Pyruvate kinase PKM	Pkm	P52480	KPYM_MOUSE	2.7	2.6
Endoplasmic reticulum chaperone BiP	Hspa5	P20029	BIP_MOUSE	2.7	2.4
Elongation factor 1-alpha 1	Eef1a1	P10126	EF1A1_MOUSE	2.7	3.9
Neutral cholesterol ester hydrolase 1	Nceh1	Q8BLF1	NCEH1_MOUSE	2.5	2.0
Actin_ cytoplasmic 2	Actg1	P63260	ACTG_MOUSE	2.5	1.4
ATP synthase subunit alpha_ mitochondrial	Atp5f1a	Q03265	ATPA_MOUSE	2.2	2.1
Antigen peptide transporter 1	Tap1	P21958	TAP1_MOUSE	2.2	2.0
Tubulin beta-5 chain	Tubb5	P99024	TBB5_MOUSE	2.1	1.7
Profilin-1	Pfn1	P62962	PROF1_MOUSE	2.1	1.7
Adenylyl cyclase-associated protein 1	Cap1	P40124	CAP1_MOUSE	2.1	1.8
Antigen peptide transporter 2	Tap2	P36371	TAP2_MOUSE	2.1	2.9

References

1. Zile, M. H. Vitamin A and Embryonic Development: An Overview. *J. Nutr.* **128**, 455–458 (1998).
2. Kiser, P. D., Golczak, M. & Palczewski, K. Chemistry of the retinoid (visual) cycle. *Chemical Reviews* **114**, 194–232 (2014).
3. Green, H. N. & Mellanby, E. Vitamin a as an anti-infective agent. *Br. Med. J.* **2**, 691–696 (1928).
4. Erkelens, M. N. & Mebius, R. E. Retinoic Acid and Immune Homeostasis: A Balancing Act. *Trends in Immunology* **38**, 168–180 (2017).
5. Iwata, M. *et al.* Retinoic acid imprints gut-homing specificity on T cells. *Immunity* **21**, 527–538 (2004).
6. Zeng, R. *et al.* Retinoic acid regulates the development of a gut-homing precursor for intestinal dendritic cells. *Mucosal Immunol.* **6**, 847–856 (2013).
7. Harrison, E. H. Mechanims of digestion and absorption of dietary vitamin A. *Annu. Rev. Nutr.* **25**, 87–103 (2005).
8. Goverse, G. *et al.* Diet-Derived Short Chain Fatty Acids Stimulate Intestinal Epithelial Cells To Induce Mucosal Tolerogenic Dendritic Cells. *J. Immunol.* **198**, 2172–2181 (2017).
9. Lampen, A., Meyer, S., Arnhold, T. & Nau, H. Metabolism of vitamin A and its active metabolite all-trans-retinoic acid in small intestinal enterocytes. *J. Pharmacol. Exp. Ther.* **295**, 979–985 (2000).
10. Molenaar, R. *et al.* Expression of Retinaldehyde Dehydrogenase Enzymes in Mucosal Dendritic Cells and Gut-Draining Lymph Node Stromal Cells Is Controlled by Dietary Vitamin A. *J. Immunol.* **186**, 1934–1942 (2011).
11. Ohoka, Y., Yokota-Nakatsuma, A., Maeda, N., Takeuchi, H. & Iwata, M. Retinoic acid and GM-CSF coordinately induce retinal dehydrogenase 2 (RALDH2) expression through cooperation between the RAR/RXR complex and Sp1 in dendritic cells. *PLoS One* **9**, 1–11 (2014).
12. Coombes, J. L. *et al.* A functionally specialized population of mucosal CD103+ DCs induces Foxp3+ regulatory T cells via a TGF-β -and retinoic acid-dependent mechanism. *J. Exp. Med.* **204**, 1757–1764 (2007).
13. Svensson, M. *et al.* CCL25 mediates the localization of recently activated CD8αβ+lymphocytes to the small-intestinal mucosa. *J. Clin. Invest.* **110**, 1113–1121 (2002).
14. Hamann, A., Andrew, D. P., Jablonski-Westrich, D., Holzmann, B. & Butcher, E. C. Role of alpha 4-integrins in lymphocyte homing to mucosal tissues in vivo. *J. Immunol.* **152**, 3282–93 (1994).
15. Pantazi, E. *et al.* Cutting Edge: Retinoic Acid Signaling in B Cells Is Essential for Oral Immunization and Microflora Composition. *J. Immunol.* **195**, 1368–1371 (2015).
16. Schambach, F., Schupp, M., Lazar, M. A. & Reiner, S. L. Activation of retinoic acid receptor-α favours regulatory T cell induction at the expense of IL-17-secreting T helper cell differentiation. *Eur. J. Immunol.* **37**, 2396–2399 (2007).
17. Benson, M. J., Pino-Lagos, K., Rosemblatt, M. & Noelle, R. J. All-trans retinoic acid mediates enhanced T reg cell growth, differentiation, and gut homing in the face of high levels of co-stimulation. *J. Exp. Med.* **204**, 1765–1774 (2007).
18. Mucida, D. *et al.* Reciprocal T H 17 and regulatory T cell differentiation mediated by retinoic acid. *Science* **317**, 256–260 (2007).
19. Sun, C.-M. *et al.* Small intestine lamina propria dendritic cells promote de novo generation of Foxp3 T reg cells via retinoic acid. *J. Exp. Med.* **204**, 1775–1785 (2007).
20. Yasgar, A. *et al.* A High-Content assay enables the automated screening and identification of small molecules with specific ALDH1A1-Inhibitory activity. *PLoS One* **12**, 1–19 (2017).
21. Niederreither, K. & Dollé, P. Retinoic acid in development: Towards an integrated view. *Nature Reviews Genetics* **9**, 541–553 (2008).
22. Fan, X. *et al.* Targeted Disruption of Aldh1a1 (Raldh1) Provides Evidence for a Complex Mechanism of Retinoic Acid Synthesis in the Developing Retina. *Mol. Cell. Biol.* **23**, 4637–4648 (2003).
23. Cravatt, B. F., Wright, A. T. & Kozarich, J. W. Activity-Based Protein Profiling: From Enzyme Chemistry to Proteomic Chemistry. *Annu. Rev. Biochem.* **77**, 383–414 (2008).
24. Liu, Y., Patricelli, M. P. & Cravatt, B. F. Activity-based protein profiling: The serine hydrolases. *Proc. Natl. Acad. Sci.* **96**, 14694–14699 (1999).
25. Koenders, S. T. A. *et al.* Development of a Retinal-Based Probe for the Profiling of Retinaldehyde Dehydrogenases in Cancer Cells. *ACS Cent. Sci.* **5**, 1965–1974 (2019).
26. Alnouti, Y. & Klaassen, C. D. Tissue distribution, ontogeny, and regulation of aldehyde dehydrogenase (Aldh) enzymes mRNA by prototypical microsomal enzyme inducers in mice. *Toxicol. Sci.* **101**, 51–64 (2008).
27. Hsu, L. C., Chang, W.-C., Hoffmann, I. & Duester, G. Molecular analysis of two closely related mouse aldehyde dehydrogenase

genes: identification of a role for Aldh1, but not Aldh-pb, in the biosynthesis of retinoic acid. *Biochem. J.* **339**, 387–395 (1999).

28. Levi, B. P., Yilmaz, Ö. H., Duester, G. & Morrison, S. J. Aldehyde dehydrogenase 1a1 is dispensable for stem cell function in the mouse hematopoietic and nervous systems. *Blood* **113**, 1670–1680 (2009).
29. Yoshida, A., Hsu, L. C. & Dave, V. Retinal oxidation activity and biological role of human cytosolic aldehyde dehydrogenase. *Enzyme* **46**, 239–244 (1992).
30. Moore, S. A. *et al.* Sheep liver cytosolic aldehyde dehydrogenase: The structure reveals the basis for the retinal specificity of class I aldehyde dehydrogenases. *Structure* **6**, 1541–1551 (1998).
31. Stagos, D. *et al.* Aldehyde dehydrogenase 1B1: Molecular cloning and characterization of a novel mitochondrial acetaldehyde-metabolizing enzyme. *Drug Metab. Dispos.* **38**, 1679–1687 (2010).
32. Grizotte-Lake, M. *et al.* Commensals Suppress Intestinal Epithelial Cell Retinoic Acid Synthesis to Regulate Interleukin-22 Activity and Prevent Microbial Dysbiosis. *Immunity* **49**, 1103–1115 (2018).
33. Mielke, L. A. *et al.* Retinoic acid expression associates with enhanced IL-22 production by γδ T cells and innate lymphoid cells and attenuation of intestinal inflammation. *J. Exp. Med.* **210**, 1117–1124 (2013).
34. Chang, F., Mahadeva, U. & Deere, H. Pathological and clinical significance of increased intraepithelial lymphocytes (IELs) in small bowel mucosa. *APMIS* **113**, 385–399 (2005).
35. Furusawa, Y. *et al.* Commensal microbe-derived butyrate induces the differentiation of colonic regulatory T cells. *Nature* **504**, 446–450 (2013).
36. Smith, P. M. *et al.* The microbial metabolites, short-chain fatty acids, regulate colonic T reg cell homeostasis. *Science* **341**, 569–573 (2013).
37. Tan, J. *et al.* Dietary Fiber and Bacterial SCFA Enhance Oral Tolerance and Protect against Food Allergy through Diverse Cellular Pathways. *Cell Rep.* **15**, 2809–2824 (2016).
38. Arpaia, N. *et al.* Metabolites produced by commensal bacteria promote peripheral regulatory T-cell generation. *Nature* **504**, 451–455 (2013).
39. Skelly, A. N., Sato, Y., Kearney, S. & Honda, K. Mining the microbiota for microbial and metabolite-based immunotherapies. *Nature Reviews Immunology* **19**, 305–323 (2019).
40. Wu, W. *et al.* Microbiota metabolite short-chain fatty acid acetate promotes intestinal IgA response to microbiota which is mediated by GPR43. *Mucosal Immunol.* **10**, 946–956 (2017).
41. Van Rooden, E. J. *et al.* Mapping in vivo target interaction profiles of covalent inhibitors using chemical proteomics with label-free quantification. *Nat. Protoc.* **13**, 752–767 (2018).
42. Rappsilber, J., Mann, M. & Ishihama, Y. Protocol for micro-purification, enrichment, pre-fractionation and storage of peptides for proteomics using StageTips. *Nat. Protoc.* **2**, 1896–1906 (2007).
43. Distler, U., Kuharev, J., Navarro, P. & Tenzer, S. Label-free quantification in ion mobility–enhanced data-independent acquisition proteomics. *Nat. Protoc.* **11**, 795–812 (2016).
44. Distler, U. *et al.* Drift time-specific collision energies enable deep-coverage data-independent acquisition proteomics. *Nat. Methods* **11**, 167–170 (2014).
45. Kuharev, J., Navarro, P., Distler, U., Jahn, O. & Tenzer, S. In-depth evaluation of software tools for data-independent acquisition based label-free quantification. *Proteomics* **15**, 3140–3151 (2015).